7
Low-mass hadrons in QCD

In this chapter we address the calculation of the properties of hadrons composed of the light quarks u, d and s.

7.1 Integrating over the fermion fields

The partition function for a fermion gauge theory

$$Z = \int DU\, D\bar{\psi} D\psi\, \exp(S_{\rm U} + S_{\rm F}) \tag{7.1}$$

can be expressed in an alternative form involving only the gauge fields by first integrating out the fermion fields. We shall use Wilson fermions as an example. We can write $S_{\rm F}$ in matrix notation,

$$\begin{aligned} S_{\rm F} &= -\sum_{x\mu} \frac{1}{2}(\bar{\psi}_x \gamma_\mu U_{\mu x} \psi_{x+\hat{\mu}} - \bar{\psi}_{x+\hat{\mu}} \gamma_\mu U^\dagger_{\mu x} \psi_x) \\ &\quad - \sum_x \bar{\psi}_x M \psi_x + \sum_{x\mu} \frac{r}{2}(\bar{\psi}_x U_{\mu x} \psi_{x+\hat{\mu}} + \bar{\psi}_{x+\hat{\mu}} U^\dagger_{\mu x} \psi_x) \qquad (7.2) \\ &\equiv -\bar{\psi} A \psi, \qquad (7.3) \\ A &= \not{D} + M - W. \qquad (7.4) \end{aligned}$$

The matrix $A = A(U)$ is called the fermion matrix. Its inverse is the fermion propagator $S(U)$ in a given gauge-field configuration,

$$S_{xy}(U) \equiv A^{-1}_{xy}(U) = \left[\frac{1}{M - W(U) + \not{D}(U)}\right]_{xy}. \tag{7.5}$$

Since ψ and $\bar{\psi}$ occur only bilinearly in the action, we can perform the integration over these variables and evaluate fermion correlation

https://doi.org/10.1017/9781009402705.008 Published online by Cambridge University Press

functions explicitly:

$$\begin{aligned} Z &= \int DU\ \det[A(U)]\ \exp(S_{\rm U}) \\ \langle \psi_x \bar\psi_y \rangle &= Z^{-1} \int DU\ \det[A(U)]\, e^{S_{\rm U}}\, S_{xy}(U) \\ &\equiv \langle S_{xy} \rangle_U, \\ \langle \psi_u \bar\psi_v \psi_x \bar\psi_y \rangle &= \langle S_{uv} S_{xy} - S_{uy} S_{xv} \rangle_U, \\ \langle \psi_u \psi_v \psi_w \bar\psi_x \bar\psi_y \bar\psi_z \rangle &= \langle S_{ux} S_{vy} S_{wz} + 5 \text{ permutations} \rangle_U, \end{aligned} \tag{7.6}$$

etc. For clarity we indicated only the space–time indices $x, \ldots$ and suppressed the color, Dirac, and flavor indices a, α, and f of the fermion fields $\psi_x^{a\alpha f}$.

7.2 Hopping expansion for the fermion propagator

For Wilson fermions an expansion in the hopping parameter $\kappa = 1/2M$ has given useful results. Here we describe it for the propagator, for which it gives an intuitive representation in terms of a summation over random paths. We have seen this earlier for the scalar field in section 3.7. Let us define the hopping matrix H by

$$H_{xa\alpha,yb\beta} = \sum_\mu [(P_\mu^-)_{\alpha\beta}\, (U_{xy})_{ab}\, \delta_{x+\hat\mu,y} + (P_\mu^+)_{\alpha\beta}\, (U_{yx})_{ab}\, \delta_{y+\hat\mu,x}], \tag{7.7}$$

in terms of which

$$A_{xa\alpha f,yb\beta g} = M_f\, \delta_{fg}\, [1 - 2\kappa_f H_{xa\alpha,yb\beta}]. \tag{7.8}$$

For a given flavor we have

$$S_{xy} = M^{-1} \left(\frac{1}{1 - 2\kappa H} \right)_{xy} = M^{-1} \sum_{L=0}^{\infty} (2\kappa)^{\rm L}\, (H^{\rm L})_{xy}, \tag{7.9}$$

where we suppressed again the non-space–time indices. The successive terms in this series can be represented as a sum over paths of length L, as illustrated in figure 7.1. The diagrams for $L+1$ are obtained from those for L by application of H (by attaching the $L = 1$ diagrams). To each path C there corresponds a color factor $U_{xy}(C)$ and a spin factor

$$\Gamma(C) = \prod_{l \in C} P_l, \tag{7.10}$$

$$P_l = P_\mu^-, \quad l = (x, x+\hat\mu) \tag{7.11}$$

$$= P_\mu^+, \quad l = (x+\hat\mu, x). \tag{7.12}$$

https://doi.org/10.1017/9781009402705.008 Published online by Cambridge University Press

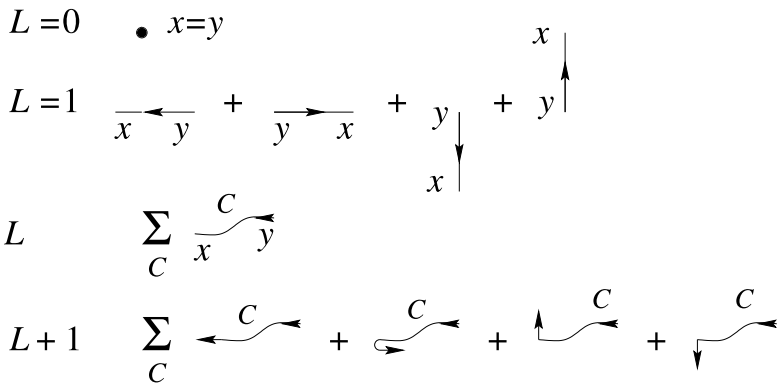

Fig. 7.1. Illustration of the terms in the hopping expansion of the propagator.

Note that, for $r = 1$, there are no paths with back-tracking because then $P^+_\mu P^-_\mu = P^-_\mu P^+_\mu = 0$.

For free fermions we can perform the summation in momentum space,

$$(H^{\mathrm{L}})_{xy} = \sum_p e^{ip(x-y)}\, H(p)^{\mathrm{L}}, \tag{7.13}$$

$$H(p)\bar{\delta}_{pq} = \sum_{xy} e^{-ipx+iqy}\, H_{xy}, \tag{7.14}$$

$$\begin{aligned} H(p) &= \sum_\mu (e^{ip_\mu}\, P^-_\mu + e^{-ip_\mu}\, P^+_\mu) \\ &= \sum_\mu (r\cos p_\mu - i\gamma_\mu \sin p_\mu), \end{aligned} \tag{7.15}$$

$$S(p) = \frac{1}{M - \sum_\mu (r\cos p_\mu - i\gamma_\mu \sin p_\mu)}. \tag{7.16}$$

So the summation over random paths with the particular weight factor (7.10) leads to the free Wilson fermion propagator. The maximum eigenvalue of $H(p)$ is $4r$ at $p = 0$, which means that the radius of convergence of the hopping expansion for free fermions is given by $|\kappa| < 1/8r$. For fixed κ and complex p the expansion diverges at the position of the particle pole in the propagator. In the interacting case the unitary $U_{\mu x}$ tend to reduce the maximum eigenvalue of H and the convergence radius is generically larger than $1/8r$, depending on the configuration of U's.

https://doi.org/10.1017/9781009402705.008 Published online by Cambridge University Press

The hopping expansion for the propagator leads to an expansion of the fermion determinant in terms of closed paths,

$$\begin{aligned}\det A \to \det(1-2\kappa H) &= \exp[\operatorname{Tr}\,\ln(1-2\kappa H)] \\ &= \exp\left[-\sum_{\mathrm{L}} \frac{(2\kappa)^{\mathrm{L}}}{L}\operatorname{Tr} H^{\mathrm{L}}\right]. \end{aligned} \tag{7.17}$$

With each closed path C there is associated a Wilson loop $\operatorname{Tr} U(C)$ and a spin loop $\operatorname{Tr}\Gamma(C)$.

7.3 Meson and baryon propagators

The expressions (7.6) are well defined without gauge fixing. Since $\int DU$ contains an implicit integration over all gauge transformations, it projects on the gauge-invariant content of the integrand. Under a gauge transformation

$$U^{\Omega}_{\mu x} = \Omega_x U_{\mu x} \Omega^{\dagger}_{x+\hat{\mu}}, \tag{7.18}$$

$$A(U^{\Omega})_{xy} = \Omega_x A(U)_{xy} \Omega^{\dagger}_y, \tag{7.19}$$

$$A^{-1}(U^{\Omega})_{xy} = \Omega_x A^{-1}(U)_{xy} \Omega^{\dagger}_y, \tag{7.20}$$

or

$$S(U^{\Omega})_{xy} = \Omega_x S(U)_{xy} \Omega^{\dagger}_y. \tag{7.21}$$

Since $\int d\Omega_x\, \Omega_x = 0$, the gauge-invariant content of Ω_x is zero and it follows that the expectation value of the gauge-field-dependent fermion propagator is zero, unless $x = y$,

$$\langle S_{xa\alpha f, yb\beta g}\rangle_U \propto \delta_{xy}\,\delta_{ab}\,\delta_{fg}. \tag{7.22}$$

The fermions cannot propagate 'on their own' without gauge fixing. Of course, this does not mean that fermion propagation is a non-gauge-invariant phenomenon and it is also not an expression of confinement. It forces us to consider carefully what the gauge-invariant description of propagation means.

A simple gauge-invariant correlation function is of the type $\langle\bar{\psi}_x\psi_x\bar{\psi}_y\psi_y\rangle$. In QCD we call these mesonic, since $\bar{\psi}\gamma\psi$ combinations carry mesonic quantum numbers. More explicitly, we can define gauge-

https://doi.org/10.1017/9781009402705.008 Published online by Cambridge University Press

invariant meson and baryon fields

$$\mathcal{M}^{\alpha f}_{x\beta g} = \delta^b_a\, \psi^{a\alpha f}_x \bar{\psi}_{xb\beta g}, \tag{7.23}$$

$$\mathcal{B}^{\alpha_1 f_1 \alpha_2 f_2 \alpha_3 f_3}_x = \epsilon_{a_1 a_2 a_3} \psi^{a_1 \alpha_1 f_1}_x \psi^{a_2 \alpha_2 f_2}_x \psi^{a_3 \alpha_3 f_3}_x, \tag{7.24}$$

$$\bar{\mathcal{B}}_{x\alpha_1 f_1 \alpha_2 f_2 \alpha_3 f_3} = \epsilon^{a_1 a_2 a_3} \bar{\psi}_{xa_1\alpha_1 f_1} \bar{\psi}_{xa_2\alpha_2 f_2} \bar{\psi}_{xa_3\alpha_3 f_3}. \tag{7.25}$$

The gauge invariance of the meson fields is obvious. For the baryon fields the effect of a gauge transformation is given by (suppressing non-color indices)

$$\begin{aligned} \epsilon_{abc}\psi^a\psi^b\psi^c &\to \epsilon_{abc}\, \Omega^a_{a'}\Omega^b_{b'}\Omega^c_{c'}\, \psi^{a'}\psi^{b'}\psi^{c'} \\ &= (\det\Omega)\, \epsilon_{a'b'c'}\, \psi^{a'}\psi^{b'}\psi^{c'}, \end{aligned} \tag{7.26}$$

and invariance follows from $\det\Omega = 1$.

By taking special linear combinations, we can construct from $\mathcal{M}$, $\mathcal{B}$, and $\bar{\mathcal{B}}$ fields with the required quantum numbers. For example, for π^+ (which has spin zero) we can use the scalar field combination

$$\bar{d}_x i\gamma_5 u_x, \quad \bar{d}_x i\gamma_\mu\gamma_5 u_x, \tag{7.27}$$

where we made flavor explicit according to

$$u^{a\alpha}_x = \psi^{a\alpha u}_x, \quad d^{a\alpha}_x = \psi^{a\alpha d}_x, \tag{7.28}$$

etc. For the ρ^+ particle (which has spin one) we can use the vector and tensor fields (both containing spin 1)

$$\bar{d}_x i\gamma_\mu u_x, \quad \bar{d}_x i[\gamma_\mu,\gamma_\nu] u_x. \tag{7.29}$$

An example for the proton (spin $\frac{1}{2}$) is given by

$$\epsilon_{abc}\,(C^\dagger\gamma_5)_{\beta\gamma}\, u^{a\alpha}_x (u^{b\beta}_x d^{c\gamma}_x - d^{b\beta}_x u^{c\gamma}_x), \tag{7.30}$$

and for the Δ^{++} (spin $\frac{3}{2}$),

$$\epsilon_{abc}\,(C^\dagger\gamma_\mu)_{\beta\gamma}\, u^{a\alpha}_x u^{b\beta}_x u^{c\gamma}_x. \tag{7.31}$$

Here C is the charge-conjugation matrix; $\bar{\psi}^{(c)} = -(C^\dagger\psi)^{\mathrm{T}}$ is the charge conjugate of $\bar{\psi}$ (cf. (D.27) in appendix D). For example, for the Δ^{++} the last two u fields combine to give a vector (containing spin 1) of the form $\bar{\psi}^{(c)}\gamma_\mu\psi$, which, together with the first u field, contains spin $\frac{3}{2}$. More examples are in [10]; [82] gives group-theoretical details of the spin–flavor content of the baryon fields.

https://doi.org/10.1017/9781009402705.008 Published online by Cambridge University Press

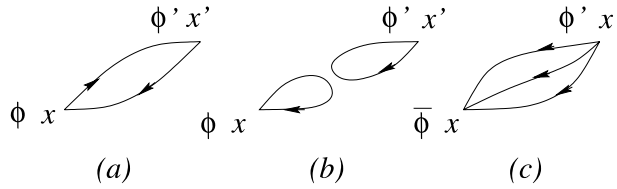

Fig. 7.2. Meson (a) and (b), and baryon (c) propagators.

Putting these hadron fields in the form ($A = \{a\alpha f\}$)

$$\mathcal{M}_x(\Phi) = \Phi^A_B \, \mathcal{M}^B_{xA}, \tag{7.32}$$

$$\mathcal{B}_x(\Phi) = \bar{\Phi}_{ABC} \, \mathcal{B}^{ABC}_x, \tag{7.33}$$

$$\bar{\mathcal{B}}_x(\Phi) = \bar{\mathcal{B}}_{xABC} \, \Phi^{ABC}, \tag{7.34}$$

where Φ specifies the spin–flavor structure, we can write gauge-invariant meson correlation functions as

$$\langle \mathcal{M}_x(\Phi) \mathcal{M}_{x'}(\Phi') \rangle = -\langle \mathrm{Tr}\,(\Phi S_{xx'} \Phi' S_{x'x}\rangle_U) + \langle \mathrm{Tr}\,(\Phi S_{xx}) \,\mathrm{Tr}\,(\Phi' S_{x'x'})\rangle_U, \tag{7.35}$$

and the baryon correlation function

$$\langle \mathcal{B}_x(\Phi) \bar{\mathcal{B}}_{x'}(\Phi') \rangle = \bar{\Phi}_{ABC} \langle S^A_{A'xx'} S^B_{B'xx'} S^C_{C'xx'} \rangle_U \Phi'^{A'B'C'}, \tag{7.36}$$

as illustrated in figure 7.2. The contribution (b) to the meson correlation function is non-zero only for flavor-neutral fields, i.e. fields of the form $\bar{f}\gamma f$, $f = u, d, c, s, t, b$.

These composite field correlation functions describe bound states, the mesons and baryons; for this reason we also call them meson and baryon propagators. Consider first the meson propagator in figure 7.2(a). It is a sum over Wilson loops going through x and x'. This follows from the hopping expansion of the quark propagator which expresses $S_{xx'}$ as a sum over random paths C weighted by the Wilson line $U_{xx'}(C)$ and the spinor factor associated with the path. We can now intuitively understand the implication of confinement as expressed by the area law for Wilson loops. The exponential fall-off in the area law greatly suppresses the contribution of widely separated paths of the two propagators in figure 7.2(a). Contributions in which the two paths stay together dominate and, when they are together, they make a random walk, which implies the formation of a bound state. A similar story can be told for the baryon propagator in figure 7.2(c); the combined random

https://doi.org/10.1017/9781009402705.008 Published online by Cambridge University Press

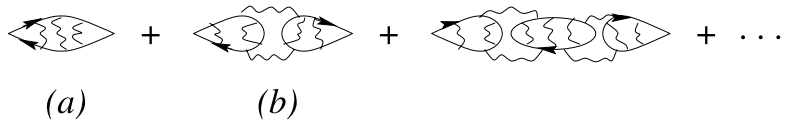

Fig. 7.3. Diagrams for flavor-neutral mesons with sea-quark loops and gluon lines also indicated.

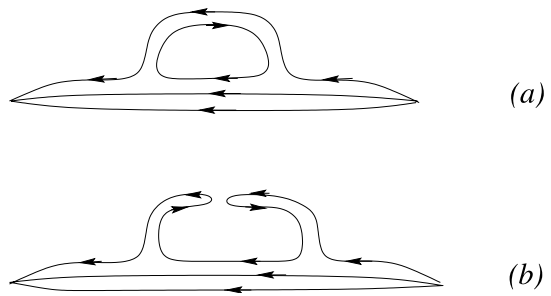

Fig. 7.4. Meson-loop corrections to the baryon propagator. The closeness of lines is to suggest binding by 'glue'.

walk of the three-quark propagators leads to a pole in momentum space corresponding to a bound baryon state.

So far we have concentrated on the fermion lines related to the hadron fields (the 'valence-quark' lines) and ignored the effect of the fermion determinant. Its hopping expansion leads to a sum of closed fermion lines called 'sea-quark' loops or 'vacuum loops', and we have to imagine such sea-quark loops everywhere in figure 7.2. This is particularly relevant for the case of flavor-neutral mesons for which diagram (b) contributes. Figure 7.3 shows diagrams (a) and (b) as the first two terms in an infinite series with the sea-quark loops included one by one. As a reminder of the presence of 'glue' implied by the average $\langle \cdots \rangle_U$ we have also shown some gluon lines in this figure. Figure 7.4 illustrates a meson-loop contribution to a baryon propagator: (a) uses a sea-quark loop but not (b), which is already included in diagram (c) of figure 7.2.

We were led by confinement to the intuitive picture of random walks for the composite hadron propagators. In a theory without confinement, such as QED, there is no area law and there will be relatively large contributions in the fermion–antifermion correlation function also for widely separated fermion paths. These will correspond to fermions propagating almost freely at large distances from each other. Of course, they will feel

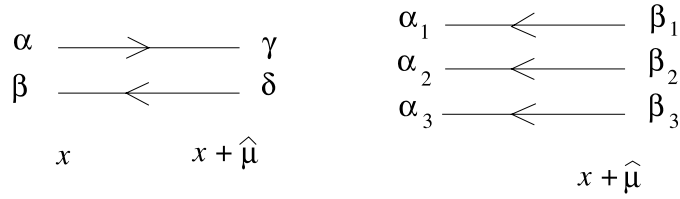

Fig. 7.5. Hopping matrix for the mesons and baryons at strong coupling.

the long range electromagnetic interactions, which may but need not lead to bound states. This is the gauge-invariant description of fermion propagation in QED.

7.4 Hadron masses at strong coupling

At bare gauge coupling $g = \infty$ the string tension diverges and there are only contributions to the Wilson paths with zero area. Neglecting vacuum fermion loops, it is an interesting approximation to take into account only simultaneous quark–antiquark hopping for mesons and three-quark hopping for baryons, as illustrated in figure 7.5. The inverse propagators can be written down explicitly and solved for the position of the pole in $p_4 = im$ at $\mathbf{p} = 0$, which determines the mass of the bound state, m. We can even derive effective actions describing the coupling constants [83, 84, 85, 109, 82] in terms of the meson and baryon fields (7.23)–(7.25). For example, the meson effective action has the form

$$S_{\text{eff}} = n_{\text{c}} \sum_x \text{Tr} \left[-\ln \mathcal{M}_x + M\mathcal{M}_x - \sum_\mu \mathcal{M}_x P_\mu^- \mathcal{M}_{x+\hat{\mu}} P_\mu^+ + O(\mathcal{M}^4) \right]. \tag{7.37}$$

where n_{c} is the number of colors and now $\mathcal{M}$ is an *effective* field. For $r = 1$ it turns out that the low-lying states are the pions, rho mesons, nucleons, and deltas ($m_\pi \approx 140$, $m_\rho \approx 770$, $m_N \approx 940$ and $m_\Delta \approx 1232$ MeV). In the flavor-degenerate case $M_u = M_d = M$ the masses are given by

$$\cosh m_\pi = 1 + \frac{(M^2-4)(M^2-1)}{2M^2-3}, \tag{7.38}$$

$$\cosh m_\rho = 1 + \frac{(M^2-3)(M^2-2)}{2M^2-3}, \tag{7.39}$$

https://doi.org/10.1017/9781009402705.008 Published online by Cambridge University Press

$$\exp m_\Delta = \frac{(M^3 - 3/2)(M^3 - 1/2)}{M^3 - 5/4}, \tag{7.40}$$

$$\exp m_N = \frac{M^3(M^3 - 2)}{M^3 - 5/4}. \tag{7.41}$$

On decreasing M from infinity toward zero or equivalently increasing the hopping parameter κ from zero upward we see that the pion mass vanishes at $M = M_c = 2$, whereas the other masses stay non-zero. At strong coupling the critical hopping parameter is $\kappa_c = 1/2M_c = \frac{1}{4}$. For weak coupling one can calculate $M_c(g) = 4 + O(g^2)$, and κ_c as defined by the vanishing of m_π will decrease toward $\frac{1}{8}$ as $g^2 \to 0$.

Although we know that the scaling region of QCD is at weak coupling, it is still interesting to compare these strong-coupling results with experiment. For small $M - M_c$,

$$m_\pi^2 = 4.8 m_q, \quad m_q \equiv M - M_c, \tag{7.42}$$

$$m_\rho = 0.894 + 1.97 m_q. \tag{7.43}$$

We can choose M such that m_π/m_ρ takes the experimental value 140 MeV/770 MeV, which gives $m_q = 0.0055$. This may be compared with $m_\rho = 0.894$ at $M = M_c$. Introducing the lattice distance, $am_\rho = 0.994$, means that the lattice cutoff is $1/a = 770/0.894 = 860$ MeV and the quark mass $m_q = 0.0055/a = 4.7$ MeV, which is remarkably close to the up–down quark mass found in numerical simulations ($m_{ud} \approx 4.5$ MeV (quenched), see section 7.5). Mass ratios not involving the pion can be approximated by taking $M = M_c$. Then we have the strong-coupling predictions

$$\frac{m_N}{m_\rho} = 1.7\ (1.21), \quad \frac{m_\Delta}{m_N} = 1.01\ (1.31), \quad M = M_c, \tag{7.44}$$

where the experimental values are given in parentheses. For $M \to \infty$ the baryon/meson mass ratio would be $\frac{3}{2}$. The results are not improved much by including $O(1/g^2)$ corrections, which are already hard to calculate [82]. The idea of using the strong-coupling expansion as a method for calculating the properties of hadrons has failed up to now because of its great complexity.

Other quantities such as the decay constants f_π and f_ρ, the π–π scattering amplitudes, and the splitting $m_\eta'^2 - (m_\eta^2 + m_{\pi^0}^2)/2$ in the neutral pseudoscalar meson sector, which is related to the notorious $U(1)$ problem, have also been calculated at strong coupling. Quantitatively these predictions are wrong of course, but they present an interesting caricature of hadron physics.

https://doi.org/10.1017/9781009402705.008 Published online by Cambridge University Press

Table 7.1. *Low-mass hadrons: the baryon octet (N, Σ, Λ, Ξ), the baryon decuplet (Δ, Σ^*, Ξ^*, Ω) and the mesons*

State	Spin	Mass (MeV)	Valence-quark content
N	1/2	940	uud, udd
Σ	1/2	1193	uus, $(ud+du)s$, dds
Λ	1/2	1116	$(ud-du)s$
Ξ	1/2	1315	uss, dss
Δ	3/2	1232	uuu, uud, udd, ddd
Σ^*	3/2	1384	uus, uds, dds
Ξ^*	3/2	1532	uss, dss
Ω	3/2	1673	sss
π	0	135	$u\bar{d}$, $d\bar{u}$
K	0	498	$u\bar{s}$, $d\bar{s}$, $s\bar{u}$, $s\bar{d}$
ρ	1	768	$u\bar{d}$, $d\bar{u}$
K^*	1	896	$u\bar{s}$, $d\bar{s}$, $s\bar{u}$, $s\bar{d}$
π^0	0	135	$u\bar{u}-d\bar{u}$ (& $s\bar{s}$)
η	0	547	$u\bar{u}+d\bar{u}-2s\bar{s}$
η'	0	958	$u\bar{u}+d\bar{u}+s\bar{s}$
ρ^0	1	768	$u\bar{u}-d\bar{u}$ (& $s\bar{s}$)
ω	1	783	$u\bar{u}+d\bar{d}$ (& $s\bar{s}$)
ϕ	1	1019	$s\bar{s}$ (& $u\bar{u}$ & $d\bar{d}$)

7.5 Numerical results

In table 7.1 the low-mass hadrons found experimentally are listed, with their valence-quark contents indicated. The electric charge of a state is just the sum of the charges of the quarks, which is $+\frac{2}{3}$ for u, $-\frac{1}{3}$ for d and s, and the opposite for the antiquarks indicated by a 'bar'. The flavor-neutral mesons (π^0, ..., ϕ) have mixed quark content, approximately as indicated (with small 'contaminations' in parentheses). The decuplet baryons are symmetric in their flavor content, whereas the octet has mixed symmetry. The neutral octet members Σ and Λ differ in the symmetry properties of their u, d flavor content. The primary aim of the numerical simulations is to recover this spectrum of hadron masses with essentially only three parameters: the Λ scale which corresponds to the gauge coupling and which sets the overall mass scale, the non-strange-quark mass in the approximation $m_u = m_d$ and the strange-quark mass m_s.

https://doi.org/10.1017/9781009402705.008 Published online by Cambridge University Press

In numerical simulations the fermion determinant $\det A$ poses the greatest problem. The *quenched approximation* consists of the replacement $\det A \to 1$, while taking its effect on the effective gauge coupling into account by a change in the bare coupling. This means that only the valence-quark propagators are taken into account and the sea-quark loops are neglected. For this reason the approximation is also called the valence approximation.

The reliability of this approximation (which destroys the Hilbert-space interpretation of the fermion path integral) is hard to establish *a priori*. It helps to consider the generalization of the $SU(3)$ gauge group to $SU(n_c)$, with $n_c \to \infty$ [67]. Then the contribution of each sea-quark loop to a mesonic correlation function is down by a factor $1/n_c$. For mesons the large-n_c limit corresponds to the quenched approximation. Baryons, however, have n_c valence quarks and the baryon mass becomes proportional to n_c as $n_c \to \infty$ [96]. Yet, as we have seen in section 5.6 for the glueballs, ordering various non-baryonic quantities according to powers of $1/n_c$ is quite illuminating even for values of n_c as low as 2 and 3.

Simulations with dynamical fermions ('unquenched') are very time consuming and for illustration we shall now describe the results of a computation with only two dynamical fermion species [97]. An improved action is used, for which larger lattice spacings can be used without discretization errors blowing up. The dynamical fermions are assumed to be the lightest sea quarks, u and d, and their masses are taken to be equal. This is not the actual situation, m_d is roughly twice m_u, both being of the order of 5 MeV.† However, the hadron masses are generally much larger and, neglecting such small $O(5\,\mathrm{MeV})$ effects, one may as well take $m_{\mathrm{sea}}^{(u)} = m_{\mathrm{sea}}^{(d)} = m_{\mathrm{sea}}$ (recall that $m \equiv M - M_c$). The pseudoscalar mesons require special attention in this respect, as will be discussed in the next chapter, but even these depend primarily on the average quark mass $(m_u + m_d)/2$. The other sea quarks in the simulation have effectively infinite mass. The masses in the valence-quark propagators can still be chosen at will; they do not have to be equal to the masses of the sea quarks, so we have $m_{\mathrm{val}}^{(ud)}$, and $m_{\mathrm{val}}^{(s)}$ as valence mass parameters for the hadrons composed of u, d and s. Such computations in which the sea-quark masses differ from the valence-quark masses are called 'partially quenched'.

In the simulations one first produces gauge-field configurations and

† This is the reason, for example, why the neutron is 1.3 MeV heavier than the proton, despite the Coulomb self-energy of the proton.

https://doi.org/10.1017/9781009402705.008 Published online by Cambridge University Press

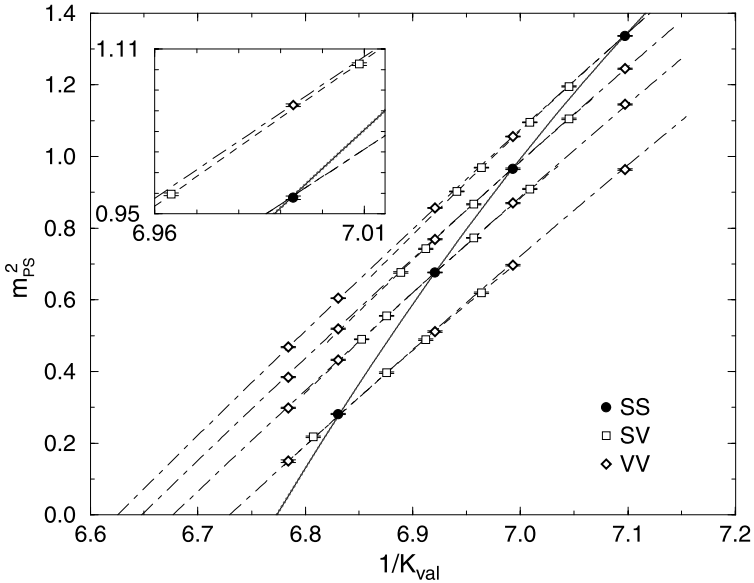

Fig. 7.6. m_{PS}^2 as a function of $1/\kappa_{\mathrm{val}}$ for $\beta = 2.1$ and four values of κ_{sea}. From [97].

then computes the average of the hadron-field correlators built from valence-quark propagators. Only valence diagrams of the type (a) in figure 7.2 are computed in this numerical study, since quark propagators corresponding to type (b) are much harder to evaluate. This means an approximation for the masses of mesons with quark–antiquarks of the same flavor (those below the second double line in table 7.1), which makes sense only if one sets $m_u = m_d$ (this follows from the discussion to be given in section 8.2). Diagrams of type (b) cause mixing of the flavor content of the mesons, which is expected to affect the vector mesons less than it does the pseudoscalars. For the η' mass diagrams of type (b) are essential.

Each choice of sea-quark mass implies a separate costly generation of gauge-field configurations, whereas the computation of valence-quark propagators is less expensive, so typically one has many more valence-quark masses than sea-quark masses available for analysis. However, by fitting suitable functions of all the masses involved, it is possible to obtain the desired mass combinations by interpolation and extrapolation. The latter is needed because the simulations need more time as the

https://doi.org/10.1017/9781009402705.008 Published online by Cambridge University Press

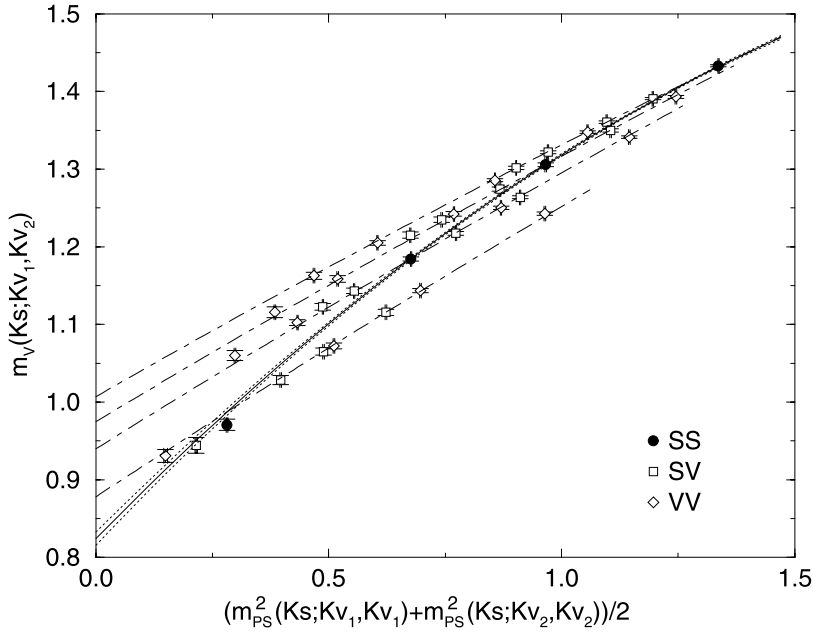

Fig. 7.7. m_{V} versus m_{PS}^2 for $\beta = 1.8$. From [97].

sea-quark masses are reduced and their small physical values cannot be simulated yet. So this introduces some uncertainty.

It turns out that the dependence of the squared pseudoscalar masses on the quark masses is almost linear, which can be understood as the result of chiral-symmetry breaking (see chapter 8), and the data can be fitted well by a quadratic polynomial in the quark masses. This is done in [97] as follows. For mesons composed of valence quarks 1 and 2 the average valence-quark mass is given by

$$m_{\mathrm{val}} = \tfrac{1}{2}\Big(m_{\mathrm{val}}^{(1)} + m_{\mathrm{val}}^{(2)}\Big), \quad m = M - M_{\mathrm{c}} = \frac{1}{2\kappa} - \frac{1}{2\kappa_{\mathrm{c}}}, \tag{7.45}$$

where κ is Wilson's hopping parameter ($r = 1$). In terms of these the pseudoscalar masses are parameterized as

$$m_{\mathrm{PS}}^2\left(\kappa_{\mathrm{sea}}; \kappa_{\mathrm{val}}^{(1)}, \kappa_{\mathrm{val}}^{(2)}\right) = b_{\mathrm{s}} m_{\mathrm{sea}} + b_{\mathrm{v}} m_{\mathrm{val}} + c_{\mathrm{s}} m_{\mathrm{sea}}^2 + c_{\mathrm{v}} m_{\mathrm{val}}^2 + c_{\mathrm{sv}} m_{\mathrm{sea}} m_{\mathrm{val}} + c_{\mathrm{vv}} m_{\mathrm{val}}^{(1)} m_{\mathrm{val}}^{(2)}. \tag{7.46}$$

In figure 7.6 results for the squared pseudoscalar masses are shown as

https://doi.org/10.1017/9781009402705.008 Published online by Cambridge University Press

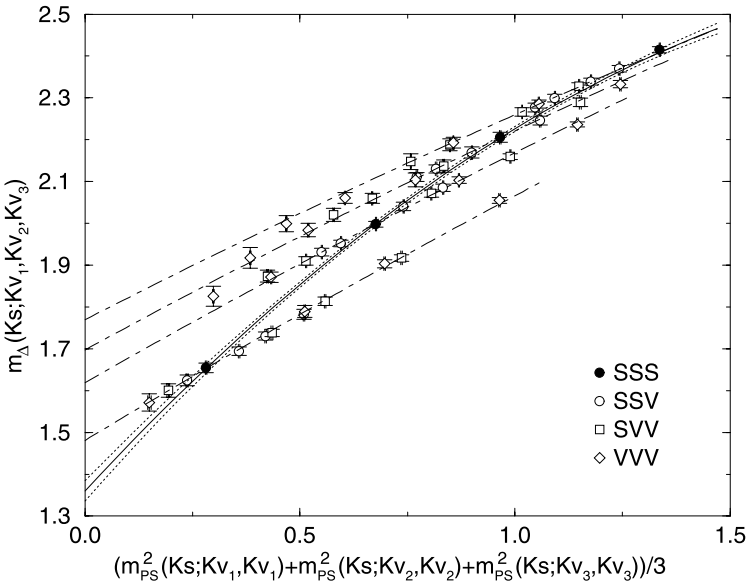

Fig. 7.8. Baryon decuplet masses versus $m^2_{\rm PS}$ for $\beta = 1.8$. From [97].

a function of the average valence-quark mass, for one of the four values $\{1.8,\ 1.95,\ 2.1,\ 2.2\}$ of the gauge coupling β used in the simulation. Results at the other β values look similar except for a change of vertical scale (the mass in lattice units being smaller at larger β). The labels 'SS', 'SV' and 'VV' mean the following.

VV: $m^{(1)}_{\rm val} = m^{(2)}_{\rm val} = m_{\rm val}$;
SV: $m^{(2)}_{\rm val} = m_{\rm sea}$; then $m^{(1)}_{\rm val}$ can be written as $m^{(1)}_{\rm val} = 2m_{\rm val} - m_{\rm sea}$;
SS: $m^{(1)}_{\rm val} = m^{(2)}_{\rm val} = m_{\rm sea}$.

The lines VV and SV almost coincide and they are almost parallel for different $\kappa_{\rm sea}$, so the line SS crosses all the others.

Note that $M_{\rm c} = 1/2\kappa_{\rm c}$ is also a free parameter in the fitting formula (7.46). If we read the right-hand side of (7.46) as a function of the inverse κ's, changing $\kappa_{\rm c}$ merely shifts all curves in figure 7.6 horizontally; $1/\kappa_{\rm c}$ is then the value at which $m^2_{\rm PS}(\kappa_{\rm crit}; \kappa_{\rm crit}, \kappa_{\rm crit}) = 0$. Knowing the parameters b_s, ..., c_{sv} and $\kappa_{\rm c}$ from the fit determines $m^2_{\rm PS}$ for every combination of the κ's and quark masses.

A similar procedure could be followed for the other hadron masses. Alternatively one can plot them as a function of $m^2_{\rm PS}$, the procedure

https://doi.org/10.1017/9781009402705.008 Published online by Cambridge University Press

followed in [97]. The vector meson masses can be fitted to a quadratic polynomial in $m_{\rm PS}^2$,

$$m_{\rm V}\left(\kappa_{\rm sea};\kappa_{\rm val}^{(1)},\kappa_{\rm val}^{(2)}\right) = A^{\rm V} + B_{\rm s}^{\rm V}\mu_{\rm sea} + B_{\rm v}^{\rm V}\mu_{\rm val} + C_{\rm s}^{\rm V}\mu_{\rm sea}^2 + C_{\rm v}^{\rm V}\mu_{\rm val}^2 + C_{\rm sv}^{\rm V}\mu_{\rm sea}\mu_{\rm val}, \quad (7.47)$$

with

$$\mu_i = m_{\rm PS}^2\left(\kappa_{\rm sea};\kappa_{\rm val}^{(i)},\kappa_{\rm val}^{(i)}\right), \quad \mu_{\rm val} = \tfrac{1}{2}(\mu_1+\mu_2), \quad (7.48)$$

$$\mu_{\rm sea} = m_{\rm PS}^2\left(\kappa_{\rm sea};\kappa_{\rm sea},\kappa_{\rm sea}\right) \quad (7.49)$$

(the data show no need for a term $C_{\rm vv}^{\rm V}\mu_1\mu_2$). A corresponding plot is shown in figure 7.7. Note the shift in vertical scale relative to figure 7.6.

Next the baryon masses are analyzed. The simplest are the decuplet states which are symmetric in the flavor indices. Writing $\mu_{\rm val} = (\mu_1+\mu_2+\mu_3)/3$, the decuplet masses can be fitted by a formula similar to (7.47), see figure 7.8. The octet baryons have a more complicated quark-mass dependence because they have a mixed flavor symmetry; we shall not go into details here (see [97]), but the corresponding figures look roughly similar to figure 7.8.

The gross features of the mass spectrum are that, for the pseudoscalars, the squared mass is approximately linear in the quark masses (and vanishing at $m_{\rm val} = m_{\rm sea} = 0$), whereas for the other hadrons the mass itself is approximately linear.

Having obtained the coefficients from the fits, the physical value of the sea-quark mass can be determined for each β. Ideally this could be done by fixing the computed pion–nucleon mass ratio at the physical value, but in this case there are good reasons to believe that the nucleon mass suffers from finite-volume effects (based on experience in previous computations). A good alternative is to use the pion–rho mass ratio. Setting $\mu_{\rm val} = \mu_{\rm sea} = m_\pi^2$ in (7.47) the equation

$$\frac{m_\pi}{A^{\rm V} + (B_{\rm s}^{\rm V} + B_{\rm v}^{\rm V})m_\pi^2 + (C_{\rm s}^{\rm V} + C_{\rm v}^{\rm V} + C_{\rm sv}^{\rm V})m_\pi^4} = \left[\frac{m_\pi}{m_\rho}\right]_{\rm phys} = 0.176 \quad (7.50)$$

can be solved for m_π.

Using $m_\rho = 768$ MeV, one can then introduce the lattice spacing a by putting $am_\rho =$ denominator in (7.50), and find the value of $1/a$ in MeV units at each β. Knowing the physical values of m_{ud} and the value of $1/a$, the masses of the nucleon and delta can be evaluated from the fits and expressed in MeV units. Linear extrapolation to zero lattice spacing

https://doi.org/10.1017/9781009402705.008 Published online by Cambridge University Press

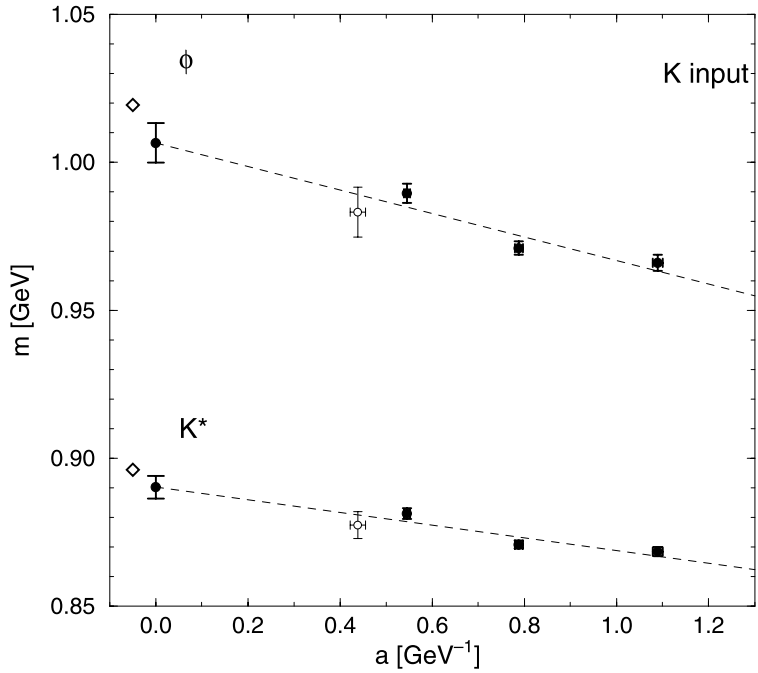

Fig. 7.9. Meson masses as a function of lattice spacing. The linear fit to $a = 0$ uses only the data at the three largest lattice spacings. Experimental values are indicated with diamonds. From [97].

(cf. figures 7.10 and 7.11) gives the results $m_N = 1034(36)$ MeV and $m_\Delta = 1392(58)$ MeV. These 'predictions' are to be compared with the experimental values of 940 and 1232 MeV (recall that in this simulation the physical volume is assumed to be somewhat small for these baryons).

Next the mass of the strange quark can be determined by fitting the kaon–rho mass ratio to the experimental value, $m^2_{\rm PS}(\kappa_{ud};\kappa_{ud},\kappa_s)/m^2_\rho = m^2_K/m^2_\rho = (498/768)^2$ (note that m_K is of the type SV). The masses of other hadrons containing strange valence quarks are then 'predictions'. Alternatively, the ϕ–ρ mass ratio was used in [97], the ϕ being of type VV, $m_{\rm V}(\kappa_{ud};\kappa_s,\kappa_s)/m_\rho = 1019/768$. The two ways of determining the valence mass of the strange quark are denoted by 'K input' and 'ϕ input'. Figure 7.9 shows such a 'prediction' for mesons as a function of the lattice spacing together with the continuum extrapolation. Examples for the baryon masses are shown in figures 7.10 and 7.11. The improved action allows rather large lattice spacings to be used. It can be seen that

https://doi.org/10.1017/9781009402705.008 Published online by Cambridge University Press

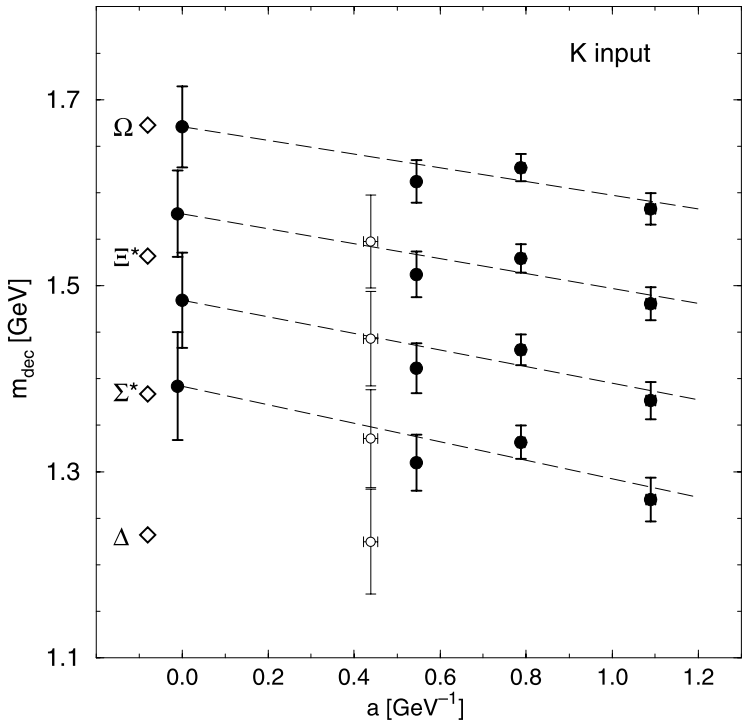

Fig. 7.10. Baryon decuplet masses as functions of a. From [97].

the a-dependence is consistent with 'linear', for the three larger lattice spacings, despite the fact that the baryon masses in lattice units are above 1 for the largest lattice spacing (cf. figure 7.8), which reduces by a factor of about two for the smallest lattice spacing.

The meson masses in the continuum limit are close to experiment at the level of 1%. The masses of baryons with three or two strange valence quarks are also close to experiment, but the discrepancy increases with only one or zero strange valence quarks. This is interpreted as finite-size effects being smaller for the hadrons involving the heavier strange valence quark (the lattice size in physical units is about 2.5 fm).

It is also of considerable phenomenological interest to determine the quark masses in physical units. In QCD the renormalized mass parameters are 'running' with the renormalization scale, similarly to the gauge coupling. An analysis of the quark masses in this simulation leads to the result $m_{ud}^{\overline{\rm MS}} \approx 3.4$ MeV and $m_s^{\overline{\rm MS}} \approx 90$ MeV, at the scale 2 GeV.

https://doi.org/10.1017/9781009402705.008 Published online by Cambridge University Press

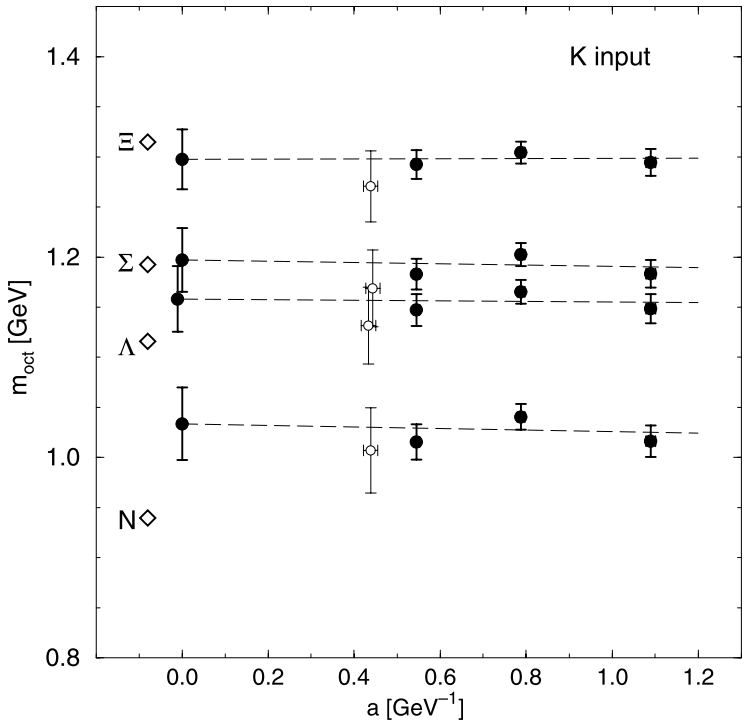

Fig. 7.11. Baryon octet masses as functions of a. From [97].

Comparing with the results of simulations in the quenched approximation, [97] finds that the inclusion of dynamical u and d quarks has improved agreement with experiment. Figure 7.12 shows a comparison; $N_{\rm f} = 2$ indicates the simulation discussed above while '$N_{\rm f} = 0$ Improved' denotes a quenched simulation using the same gauge-field action; '$N_{\rm f} = 0$ Standard' shows the results of an earlier simulation [98] using the standard Wilson action. It is surprising how good the quenched approximation actually is for the hadron spectrum. The effect of dynamical fermions on various physical quantities is not easily established, see e.g. [99]. One may expect that results will further improve with simulations including also a dynamical strange quark, as well as including larger volumes.

https://doi.org/10.1017/9781009402705.008 Published online by Cambridge University Press

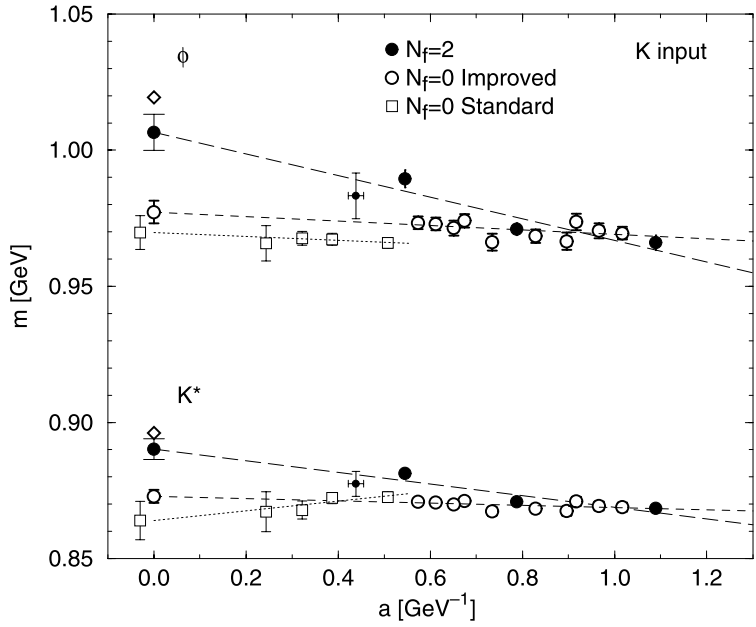

Fig. 7.12. A comparison with the quenched approximation. From [97].

7.6 The parameters of QCD

The parameters in the Wilson action ($r = 1$) are g^2 and $m_f = M_f - M_c$, the critical value $M_c = 1/2\kappa_c$ being determined completely by the gauge coupling. We have seen in the previous sections how these may be determined by the hadron spectrum. In particular, g^2 determines the overall scale, say the proton mass m_p at $m_u = m_d = m_s = 0$, while the quark masses determine the ratios m_{PS}^2/m_p^2. Roughly speaking, m_p, m_{π^+}, m_{K^+}, and m_K^0 are the free parameters of three-flavor QCD.

The renormalized masses and coupling depend in general on the renormalization scheme. In a mass-independent scheme such as minimal subtraction (cf. problem (iii) for a perturbative lattice definition), we get renormalized running coupling and masses at momentum scale μ, $\bar{g}(\mu)$ and $\bar{m}_f(\mu)$. They satisfy the renormalization-group equations

$$\mu \frac{d\bar{g}}{d\mu} = \beta(\bar{g}), \quad \mu \frac{d\bar{m}_f}{d\mu} = \gamma(\bar{g})\,\bar{m}, \tag{7.51}$$

https://doi.org/10.1017/9781009402705.008 Published online by Cambridge University Press

with†

$$\beta(\bar{g}) = -\beta_1 \bar{g}^3 - \beta_2 \bar{g}^5 - \cdots, \tag{7.52}$$

$$\gamma(\bar{g}) = -\gamma_1 \bar{g}^2 - \gamma_2 \bar{g}^4 - \cdots. \tag{7.53}$$

Here β_1, β_2 and γ_1 are universal and given by

$$\beta_1 = \frac{1}{16\pi^2}\left(\frac{11}{3}n_{\rm c} - \frac{2}{3}n_{\rm f}\right), \tag{7.54}$$

$$\beta_2 = \frac{1}{(16\pi)^2}\left[\frac{34}{3}n_{\rm c}^2 - \frac{10}{3}n_{\rm c}n_{\rm f} - \frac{(n_{\rm c}^2-1)n_{\rm f}}{n_{\rm c}}\right], \tag{7.55}$$

$$\gamma_1 = \frac{1}{16\pi^2}\,\frac{3(n_{\rm c}^2-1)}{n_{\rm c}}, \tag{7.56}$$

where $n_{\rm c}$ is the number of colors and $n_{\rm f}$ the number of dynamical flavors.

We have already seen in section 5.2 how an overall scale Λ may be defined in terms of the gauge coupling,

$$\Lambda = \mu(\beta_1\bar{g}^2)^{-\beta_2/2\beta_1^2} e^{-1/2\beta_1\bar{g}^2} \times \exp\left\{-\int_0^{\bar{g}} dg\left[\frac{1}{\beta(g)} + \frac{1}{\beta_1 g^3} - \frac{\beta_2}{\beta_1^2 g}\right]\right\}. \tag{7.57}$$

This scale is *renormalization-group invariant*, i.e. $d\Lambda(\mu, \bar{g}(\mu))/d\ln\mu = 0$. Similarly one defines renormalization-group-invariant quark masses

$$m_f^{\rm rgi} = \bar{m}_f(\mu)(2\beta_1\bar{g}^2)^{-\gamma_1/2\beta_1} \times \exp\left\{-\int_0^{\bar{g}} dg\left[\frac{\gamma(g)}{\beta(g)} - \frac{\gamma_1}{\beta_1 g}\right]\right\}, \tag{7.58}$$

which satisfy $dm_f^{\rm rgi}(\mu, \bar{g}(\mu))/d\ln\mu = 0$. As we have seen in section 5.2, the scale Λ depends on the renormalization scheme; however, using similar arguments it follows that the $m_f^{\rm rgi}$ are scheme-independent. In [63] special techniques are used to compute the renormalization-group functions $\beta(g)$ and $\gamma(g)$ non-perturbatively.

Asymptotic freedom ($\beta_1 > 0$) is guaranteed for $n_{\rm f} < 11n_{\rm c}/2$, or $n_{\rm f} \leq 16$ for QCD. We also see from the μ-independence of $\bar{m}_f^{\rm rgi}$ that the running mass $\bar{m}_f(\mu)$ goes to zero $\propto (\bar{g}^2)^{\gamma_1/2\beta_1}$ as $\mu \to \infty$. The same is true for the bare quark mass m_f as the lattice spacing $a \to 0$ (in minimal subtraction the bare parameters run in the same way the renormalized ones, cf. problem (iv)).

† The subscript k of β_k and γ_k indicates that the coefficient corresponds to diagrams with k loops. Another notation, often used, is $\beta_k \to \beta_{k-1}$, $\gamma_k \to \gamma_{k-1}$, and [63] $\beta_k \to b_{k-1}$, $k = 1, 2, \ldots$, $\gamma(\bar{g}) \to \tau(\bar{g}) = -d_0\bar{g}^2 - d_1\bar{g}^4 - \cdots$.

https://doi.org/10.1017/9781009402705.008 Published online by Cambridge University Press

7.7 Computing the gauge coupling from the masses

At long distances the non-perturbative methods of lattice gauge theory allow us to compute the properties of hadrons. At short distances we know that weak-coupling perturbation theory works well. Many physical properties have been successfully related with the methods of perturbative QCD. The essential parameter in these calculations is the renormalized coupling constant $g_{\rm R}$. A useful characterization of the coupling strength is the value of the running coupling $g_{\overline{\rm MS}}(\mu)$ in the $\overline{\rm MS}$ scheme, which is customarily taken at the scale set by the mass of the Z-boson, $\mu = m_Z$, or rather the value of the 'strong fine-structure constant' $\alpha_{\rm s}(m_Z) = g^2_{\overline{\rm MS}}(m_Z)/4\pi$. It is not a free parameter; its value can be predicted just like other physical quantities such as mass ratios. Let us see in more detail how this can be done.

Suppose that we compute the static quark–antiquark potential V at short distances. From the force

$$F(r) = \frac{\partial V}{\partial r} = C_2\,\frac{g^2_{\rm V}(1/r)}{4\pi r^2}, \tag{7.59}$$

we know $g^2_{\rm V}(1/r)$ at some distance r/a in lattice units, for some bare g and quark-mass parameters aM, chosen such that m_π/m_p, m_K/m_p, ... have the experimental values to reasonable accuracy. From the value of the proton mass in lattice units, am_p, we then also know the distance r in units of m_p, rm_p. Provided that rm_p is small enough, we can then use the perturbative renormalization group

$$\frac{\mu\, dg_{\rm V}}{d\mu} = \beta(g_{\rm V}), \quad \beta(g_{\rm V}) = -\beta_1 g^3_{\rm V} - \beta_2 g^5_{\rm V} + \cdots, \quad \mu = 1/r, \tag{7.60}$$

to relate the computed $g^2_{\rm V}(1/r)$ to $g^2_{\rm V}$ at higher μ. At sufficiently large μ we can use the perturbative connection between $g^2_{\rm V}$ and $g^2_{\overline{\rm MS}}$ parameterized by the ratio of the scales $\Lambda_{\overline{\rm MS}}/\Lambda_{\rm V}$.

This program is difficult to implement because the lattices for simulations with dynamical fermions in spectrum computations tend to be small. Other renormalized coupling constants have been proposed in place of $g_{\rm V}$, which are useful for numerical computations, e.g. the 'Schrödinger functional method' [94].

7.8 Problems

(i) *Effective action*

The exponent in (7.17) can be interpreted as an effective action

https://doi.org/10.1017/9781009402705.008 Published online by Cambridge University Press

for the gauge field. Calculate the contribution of the smallest closed loop (around a plaquette). Show that it corresponds to an *decrease* (i.e. increase of the effective $\beta = 6/g^2$) of the effective gauge coupling.

(ii) *Three flavors*
Devise a method for analyzing numerical hadron-mass data with dynamical up, down and strange quarks, with $m_u = m_d \neq m_s$.

(iii) *Minimal subtraction revisited*
In the following g_0 and m_0 denote the bare gauge coupling and quark masses, and g and m the renormalized ones (we suppress the flavor label f). For Wilson fermions $m_0 \equiv M - M_c(g_0, r)$. For staggered fermions we may think of m_0 simply being the parameter appearing in the action (see [73] for more details). The critical mass M_c is linearly divergent and the bare m_0 has to absorb the remaining logarithmic divergences as the lattice spacing $a \to 0$. The coupling g_0 is logarithmically divergent. We shall now follow similar steps to those in problem 3(iv) for the QCD case.

Both g_0 and m_0 are multiplicatively renormalized,

$$g_0 = g Z_g(g, \ln a\mu), \tag{7.61}$$

$$m_0 = m Z_m(g, \ln a\mu), \tag{7.62}$$

$$\begin{aligned} Z_g(g, \ln a\mu) &= 1 + \sum_{n=1}^{\infty} \sum_{k=0}^{n} Z_{nk}^g g^{2n} (\ln a\mu)^k \\ &= \sum_{k=0}^{\infty} Z_k^g(g) (\ln a\mu)^k, \end{aligned} \tag{7.63}$$

and similarly for Z_m,

$$Z_m(g, \ln a\mu) = \sum_{k=0}^{\infty} Z_k^m(g) (\ln a\mu)^k. \tag{7.64}$$

Terms vanishing as $a \to 0$ have been neglected, order by order in perturbation theory. In principle we can allow any choice of the coefficients $Z_{nk}^{g,m}$ which lead to a series in g^2 for the renormalized vertex functions in which the dependence on a cancels out. In minimal subtraction one chooses

$$Z_0^g(g) \equiv 1, \quad Z_0^m(g) \equiv 1. \tag{7.65}$$

The renormalized g and m depend on the physical scale μ but not on a whereas g_0 and m_0 are supposed to depend on a but not

https://doi.org/10.1017/9781009402705.008 Published online by Cambridge University Press

on μ. Then

$$0 = \left[\mu \frac{\partial}{\partial \mu} + \beta(g) \frac{\partial}{\partial g}\right] g Z_g(g, \ln a\mu), \tag{7.66}$$

$$0 = \left[\mu \frac{\partial}{\partial \mu} + \beta(g) \frac{\partial}{\partial g} + \gamma(g)\right] Z_m(g, \ln a\mu), \tag{7.67}$$

where

$$\beta(g) = \mu \frac{dg}{d\mu}, \quad \gamma(g) = \frac{\mu}{m} \frac{dm}{d\mu}. \tag{7.68}$$

By going through similar arguments to those in problem 3(iv), show that in minimal subtraction

$$\beta(g) = -Z_1^g(g), \quad \gamma(g) = -Z_1^m(g). \tag{7.69}$$

Verify that, in minimal subtraction, the renormalization-group functions for the bare parameters are identical to those for the rernormalized ones, $\beta_0(g_0) = \beta(g_0)$ and $\gamma_0(g_0) = \gamma(g_0)$. Verify the RG-independence of Λ and $m^{\rm rgi}$ in (7.57) and (7.58).

https://doi.org/10.1017/9781009402705.008 Published online by Cambridge University Press